Improved identification of a blade-disk coupling through a parametric study of the dynamic hybrid models

(Article begins on next page)

24 April 2024

Improved identification of a blade-disk coupling through a parametric study of the dynamic hybrid models

Z. Saeed, M. Kazeminasab, C. M. Firrone, T. M. Berruti
Department of Mechanical Engineering, Politecnico di Torino,
Corso Duca degli Abruzzi 24, 10129, Turin, Italy
e-mail: **zeeshan.saeed@polito.it**

Abstract

Joint identification of blade-root joints in typical bladed-disk assemblies is not possible with the classic decoupling methods due to inaccessibility of interface degrees-of-freedom. In a recent study, an attempt was made to identify such a joint by an expansion based decoupling strategy called System Equivalent Model Mixing (SEMM). The expanded sub-models of the connected substructures and their assembly can be influenced by the measurement errors and the discrepancies between the numerical and experimental sub-models. Therefore, the accuracy of the identified joint is compromised. In this work, we investigate some key factors to improve the expanded sub-models through a new measurement campaign on the unconstrained substructures and the assembly. These factors are i) expansion error, ii) interface type, and iii) singular value filtering. The resulting identified joint properties are validated by recoupling the joint with the respective substructures. It is shown that, by controlling these factors, the joint identification can be highly improved.

1 Introduction

Bladed-disks are critical structural components in turbomachines for adding or extracting mechanical energy to or from the surrounding fluid. The blades are subjected to high dynamic forces which can cause their failure due to high cycle fatigue. Their accurate response prediction is, therefore, necessary in the design phase. A typical bladed-disk assembly includes multiple joints (blade-root, shroud, under-platform etc.) [1, 2]. The joints might be beneficial in regards to the friction damping [1], however, they introduce uncertainty and variability even for linear response prediction in the assembly. The problem becomes even more challenging as the interfaces in the bladed-disk joints are small, intricate and inaccessible for measurements. In order to predict the assembly's dynamics (considering typical non-rigid connections), the joint dynamics have to be estimated or measured. This can be achieved by the reverse approach i.e. by decoupling the known subsystems from the known assembled system [3, 4].

The decoupling of the known subsystems requires knowledge of the interface dynamics. Since the joint interfaces in the blade-roots are not accessible for measurements, the dynamics have to be expanded there. For this purpose, the technique System Equivalent Model Mixing (SEMM) [5] can be used to produce a frequency-domain hybrid model with the expanded dynamics. Essentially, the method mixes different model descriptions (numerical and experimental) of a component. These expanded dynamics in the substructures, if predicted accurately, can then be decoupled from the assembled system's measured dynamics to identify the joint – since the joint can be seen as the difference between the assembly and the associated substructures. The identification of the joint can be done by the decoupling methods based on a primal formulation [6–9]. However, the cited methods have been used on relatively simpler joint interfaces.

Using the idea of dynamic expansion (by SEMM) also to the assembly, an iterative decoupling strategy was proposed in [10] to identify the joint dynamics. The method was recently applied to a blade-root joint of an academic bladed-disk in [11]. However, the actual joint identification was marginally successful in a localized frequency band. Since the method is based on Frequency Based Substructuring (FBS) [12], it is likewise sensitive to measurement inaccuracies [13–15] as well as the expansion error.

In this paper, we investigate some of the key factors that affect the expansion (SEMM) based joint identification method on the same test-case as examined in [11]. The factors considered are: i) expansion error, ii) interface description and iii) singular value (SV) based filtering. They encompass the substructure hybrid models (substructures) and the connections between them (the interface) which are essential elements in the decoupling (or coupling) process. First, the expansion error is reduced by performing a new measurement campaign on the substructures in free boundary conditions as well as the assembly to produce better hybrid models. In fact, the modelling discrepancies posed by the constraints caused a high expansion error in [11]. Secondly, different interface (connection points) variants are studied to know which locations and which joint model size is appropriate to accurately predict the assembled system's dynamics. Thirdly, the singular value filters are used to reduce noise in the hybrid models' quality. The SV filters in SEMM were introduced for the first time in [16] on a single substructure level. They are applied here in the context of joint identification. The results show that in order to achieve a good joint identification, these factors play an important role and must be considered in this expansion based joint identification method.

The paper is organized as follows: the theoretical and mathematical background is briefly reviewed in Section 2. The measurement campaign, the experimental model details and low expansion error effects are discussed in Section 3. The results of effects of interface types and singular value filtering on the joint identification are presented in Section 4 and Section 5, respectively. The paper is then concluded in Section 6.

2 Theoretical Background

In this section, we briefly write the key sets of equations used in the analysis. For more details, the readers can refer to the related previous work and the cited literature. Frequency based Substructuring (FBS) [12] provides a convenient framework to couple substructures. Consider two substructures A and B with their receptance (or accelerance) expressed as $\mathbf{Y}^A$ and $\mathbf{Y}^B$, respectively, can be coupled by the Lagrange multiplier FBS [17] form:

$$\mathbf{Y}^{AB} = \mathbf{Y} - \mathbf{Y}\mathbf{B}^T(\mathbf{B}\mathbf{Y}\mathbf{B}^T)^{-1}\mathbf{B}\mathbf{Y} \quad \text{with} \quad \mathbf{Y} = \begin{bmatrix} \mathbf{Y}^A & \\ & \mathbf{Y}^B \end{bmatrix} \tag{1}$$

where $\mathbf{B}$ is the signed Boolean matrix to make the interface displacements compatible. If $\mathbf{B}$ is appropriately defined, the receptance for coupling $\mathbf{Y}^{AB}$ in Eq. (1) is expressed in the compact notation as:

$$\mathbf{Y}^{AB} = fbs(\mathbf{Y}^A, \mathbf{Y}^B). \tag{2}$$

Similarly, it can also be used to decouple a substructure from a known coupled system to identify the dynamics of the unknown subsystem [3,4]. In order to identify a joint $\bar{\mathbf{Y}}^J$ in an assembled system $\mathbf{Y}^{AJB}$, the subsystems $\mathbf{Y}^A$ and $\mathbf{Y}^B$ are decoupled as negative substructures:

$$\bar{\mathbf{Y}}^J = fbs(\mathbf{Y}^{AJB}, -\mathbf{Y}^A, -\mathbf{Y}^B). \tag{3}$$

In Eq. (2)–(3), square FRF matrices of the structures are required which may not be practically feasible in an experiment. Consider the substructure A whose FRF matrix is square consisting of FRFs on the internal $(\star)_i$ and boundary $(\star)_b$ DoF.

$$\mathbf{Y}^A = \begin{bmatrix} \mathbf{Y}_{ii} & \mathbf{Y}_{ib} \\ \mathbf{Y}_{bi} & \mathbf{Y}_{bb} \end{bmatrix}^A \tag{4}$$

In many cases, the boundary or interface DoF are not accessible for measurements. This implies that only $\mathbf{Y}_{ii}^A$ can be obtained by measurements. Even so, it would not be possible to measure all the elements of this matrix. Therefore, we further divide the FRF matrix $\mathbf{Y}_{ii}^A$ into:

$$\mathbf{Y}_{ii}^A = \begin{bmatrix} \mathbf{Y}_{cc} & \boxed{\mathbf{Y}_{ce}} & \mathbf{Y}_{co} \\ \mathbf{Y}_{ec} & \mathbf{Y}_{ee} & \mathbf{Y}_{eo} \\ \mathbf{Y}_{oc} & \mathbf{Y}_{oe} & \mathbf{Y}_{oo} \end{bmatrix}^A \tag{5}$$

The different subscripts denote the DoF sets where:

$(\star)_c$: displacements are measured

$(\star)_e$: excitations are applied

$(\star)_o$: one or both of the above can be measured – to be reserved for validation.

Based on these definitions, in Eq. (5), the diagonal blocks contain the drive-point FRFs which are difficult to measure in practice. The FRF blocks shown in the box in Eq. (5) are more feasible and easy. This means that the sensors and impacts are not collocated and overdetermined (non-square) FRF matrices can be measured. The remaining matrix blocks may not be possible to measure due to practical limitations.

2.1 Experimental Model

The FRFs $\mathbf{Y}_{ce}^A$ are more practical and convenient for measurements, as discussed above. We choose $\mathbf{Y}_{ce}^A$ to be our experimental model denoted by $\mathbf{Y}^{\text{ov},A}$. This model is measured on the internal DoF of substructure A and then used for expansion on its interface DoF.

2.2 Numerical Model

A numerical FRF model obtained from a Finite Element (FE) analysis can provide the FRFs for all the DoF including the ones inaccessible (interface) and inconvenient (drive-point) for measurement. It can then provide all the elements in the FRF matrices of Eq. (4) and (5). This model is denoted by $\mathbf{Y}^{\text{N},A}$. Note that some discrepancies in modelling always exist between the numerical and experimental models.

2.3 Hybrid Model by SEMM

Using the above two models, one can construct a hybrid model by System Equivalent Model Mixing (SEMM) [5]. The method uses the DoF structure of the numerical model $\mathbf{Y}^{\text{N},A}$ and overlays the measured dynamics of the experimental model $\mathbf{Y}^{\text{ov},A}$. The resulting hybrid or expanded model $\mathbf{Y}^{\text{S},A}$ is computed by the following expression:

$$\mathbf{Y}_{gg}^{\text{S},A} = semm(\mathbf{Y}^{\text{N},A}, \mathbf{Y}^{\text{ov},A}) = \mathbf{Y}_{gg}^{\text{N},A} - \mathbf{Y}_{gg}^{\text{N},A}(\mathbf{Y}_{cg}^{\text{N},A})^+ (\mathbf{Y}_{ce}^{\text{N},A} - \mathbf{Y}^{\text{ov},A})(\mathbf{Y}_{ge}^{\text{N},A})^+ \mathbf{Y}_{gg}^{\text{N},A} \quad (6)$$

where $(\star)^+$ denotes the pseudo-inverse and $(\star)_{gg}$ the set of all the DoF i.e. $g = \{i, b\} = \{c, e, o, b\}$. Thus, the dynamics on the interface of substructure A are obtained through expansion by Eq. (6) in $\mathbf{Y}^{\text{S},A}$. Similarly, the hybrid models $\mathbf{Y}^{\text{S},B}$ for substructure B and $\mathbf{Y}^{\text{S},AJB}$ for the coupled system AJB can also be obtained, if their respective numerical models are viable. The use of J here is to emphasize an explicit presence of the joint dynamics in the assembly.

Remark 1. *The pseudo-inverses in Eq. (6) can be computed by singular value decomposition (SVD). This allows to filter the lowest singular values. This effect on the hybrid models of a single substructure have been studied in [16]. The resulting models are called the filtered hybrid models and their effect on the joint identification is discussed here in Section 5.*

2.4 Joint Identification by SEMM

Using the hybrid models of the substructures A and B and measured dynamics $\mathbf{Y}^{\text{ov},AB}$ on the assembled (built-up) system AB, the coupled hybrid models can be created. In order to identify the joints dynamics, an iterative method was proposed in [10] and applied to a real geometry in [11]. Here only the essential steps are briefly recapitulated.

1. Construct hybrid models of substructures A and B, denoted by $\mathbf{Y}^{\text{S},A}$ and $\mathbf{Y}^{\text{S},B}$, respectively.
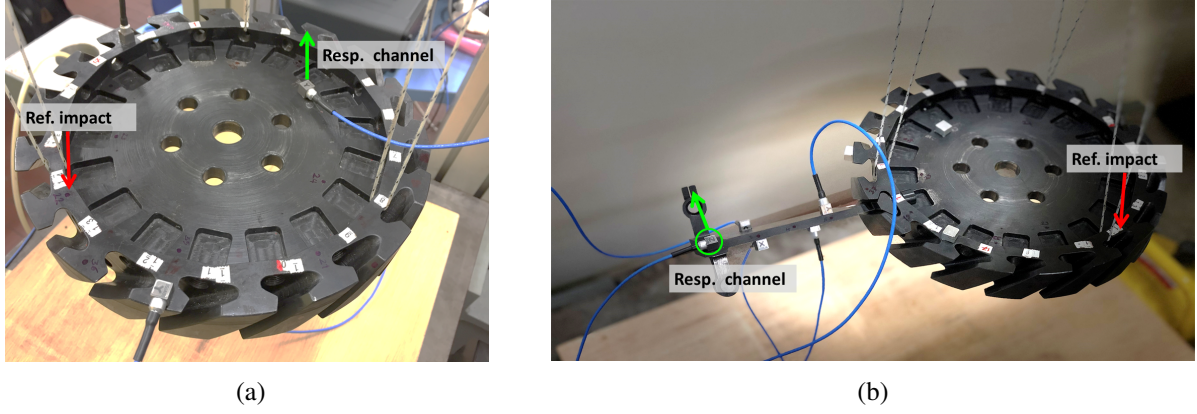
<div align="center">(a)   (b)</div>

Figure 1: Setup for FRF measurements on (a) the disk and (b) the blade-disk assembly. Due to limited DAQ channels availability, the assembly measurements were carried out in two steps. The picture of the assembly (b) shown is one of those steps in which the sensors are mounted on the blade. The dummy masses are installed on the disk to cancel out the mass effect in the joint decoupling. The arrows represent the locations of reference FRF measurements for validation.

2. Measure FRFs on the built-up system AB in which the joint dynamics are sufficiently observed.

3. Create the numerical model of the coupled system AJB with nth joint dynamics $\mathbf{Y}_n^J$:

$$\mathbf{Y}_n^{\text{N},AJB} = fbs(\mathbf{Y}^{\text{S},A}, \mathbf{Y}_n^J, \mathbf{Y}^{\text{S},B}) \tag{7}$$

4. Generate the coupled hybrid model

$$\mathbf{Y}_n^{\text{S},AJB} = semm(\mathbf{Y}_n^{\text{N},AJB}, \mathbf{Y}^{\text{ov},AB}). \tag{8}$$

5. Identify the joint by FBS decoupling

$$\mathbf{Y}_{n+1}^J = fbs(\mathbf{Y}_n^{\text{S},AJB}, -\mathbf{Y}^{\text{S},A}, -\mathbf{Y}^{\text{S},B}). \tag{9}$$

6. Update the coupled numerical model $\mathbf{Y}_{n+1}^{\text{N},AJB}$ in step 3 with $\mathbf{Y}_{n+1}^J$ until the expansion error decreases below a set tolerance or remains unchanged for at least 03 iterations.

Remark 2. *While computing $\mathbf{Y}_n^{\text{S},AJB}$ in Eq. (8) through Eq. (6), the inverses are computed by weighted pseudo-inverses, for example, for a matrix $\mathbf{P}$*

$$\mathbf{P}^+ = (\mathbf{P}^T\mathbf{W}\mathbf{P})^{-1}\mathbf{P}^T\mathbf{W} \tag{10}$$

where $\mathbf{W}$ is a diagonal weighting matrix assigning higher weights to some DoF. This was shown on an assembly of a blade and disk in [11] by assigning higher weights to the boundary DoF. This resulted in a decrease in the subsystem internal effects and an improvement of the convergence. The same or a greater order of weights (1×10^{10}) was applied for the joint identification in this paper.

3   The Test Campaign

In this section, the measurement campaign on the test geometries of a blade, disk, and their assembly connected through a dove-tail joint are described. Since this type of interface is not accessible for measurements, FRFs at the interfaces are predicted by the SEMM expansion. The same test-case was studied by these authors in [11] with a fixed constraint on the disk (and also on the assembly). The constraint seemed to greatly

Table 1: Measurement channels and models details for the joint identification

Description	Blade A	Disk B	Assembly AB
Number of response channels (α)	15	15	30
Number of impacts (β)	18	19	37
Experimental validation channels	–	Figure 1a	Figure 1b
Total internal DoF ($\gamma = \alpha + \beta$)	33	34	67
Size of experimental FRF matrix $\mathbf{Y}^{\mathrm{ov}}$	14×18	14×19	27×36 [a]
Number of Boundary DoF [b]	27	27	–
Size of numerical FRF matrix	60×60	61×61	– [c]
Size of hybrid FRF matrix (before VP transformation)	60×60	61×61	–

[a]One sensor channel had unusually high noise and it had to be discarded, therefore, the experimental FRF matrices are one channel short for the blade and disk and two channels short for the assembly. However, one response channel and one input channel was additionally left out for the validation in the assembly

[b]These DoF are inaccessible and expanded over. Some or all of the boundary DoF are then used to represent the interface in Section 4

[c]The size of the coupled system depends on the interface type discussed in Section 4 and the formulation in FBS (primal or dual).

affect the joint identification results. In this work, the fixed constraint has been removed and so the FRFs have been measured in free conditions, as shown in Figure 1. Consequently, the modelling and expansions errors caused by the constraint are reduced. However, other modelling errors, for example, FE model updating or non-coincident DoF in experimental and numerical models, are unavoidable.

Figure 1 shows the sensors (triaxial accelerometers) and impacts positions for reference (validation) measurements. The readers can refer to [11] for their locations, as they have been kept the same in this new test campaign. Some key details regarding the experimental setup and the different models are presented in Table 1.
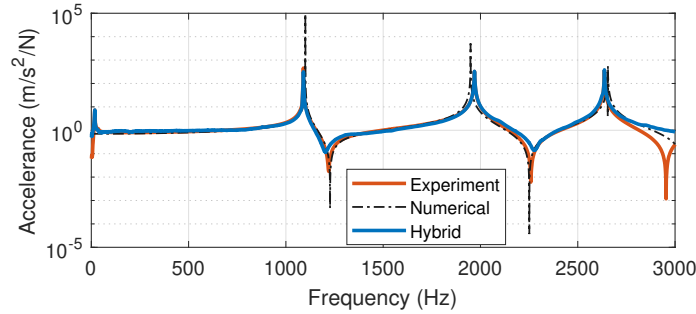

Figure 2: Validation of SEMM on the disk. The output/input locations of these FRFs are indicated in Figure 1a.

Before proceeding for the joint identification from the assembly, the effectiveness of the SEMM expansion is first checked at the substructure level. The method is tested on the disk which has been modelled and tested in free boundary conditions, as mentioned above. In Figure 2, three FRFs are plotted. The numerical (black dotted) FRF agrees well with the the experimental FRF (reference) despite having no damping and slight differences at the resonances. Comparing these disk FRFs with those in [11], such agreement was achieved by removing the constraint and updating the material properties in the FE model. The hybrid FRF obtained by SEMM – using an overlay model without the reference FRF – predicts those resonance peaks exactly. Some differences in the anti-resonances are attributed to the unavoidable errors in the FRF output or input locations while conducting tests. This expansion in the disk FRFs is certainly more reliable than with the
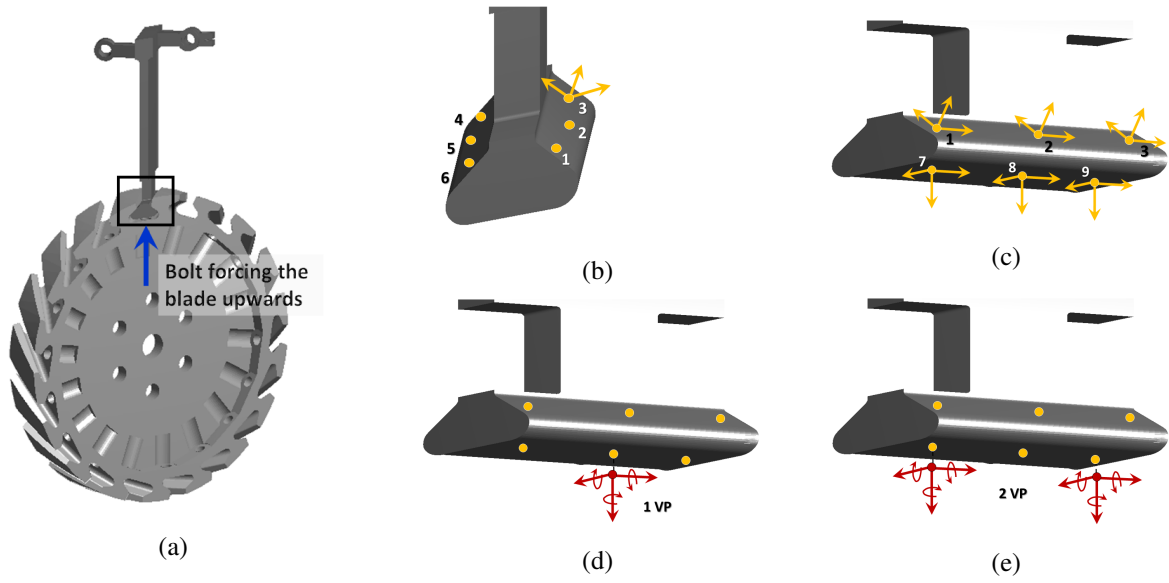
Figure 3: Different representations of interface DoF on the blade. (a) Assembled blade and disk depicting the connection (b) Left and right surfaces on the blade interface with three translational DoF per node. (c) Another view of the blade interface indicating additional three nodes on the bottom surface. (d) One virtual point interface formed by transforming all the translational DoF on nodes 1 through 9. There are six DoF per virtual point. (e) Two virtual point interface.

fixed constraint in [11]. As a results, it should improve identifiability of the joint.

In the next sections, the linear joint dynamics are identified by varying different parameters. In detail, these parameters are the description of interface (Section 4) and singular value filtering in the substructure hybrid models (Section 5). In each case, the same method of Section 2.4 is used. The weights mentioned in Remark 2, have been used on the boundary DoF to avoid the influence of internal subsystem resonances on the joint identification.

4 Effect of Interface Type on the Identification

An interface provides the links or paths through which the dynamic coupling between substructures is established. The more accurately they are measured or expanded, the more accurate will be the coupled system's predicted dynamics (also for the decoupling or joint identification). Therefore, it is essential that the interface is described appropriately. In this section, different cases of interface modelling based on different discretization are studied on the blade and disk assembly in the context of joint identification. For a fair comparison of different interfaces, the identified joint dynamics are not compared with each other as the joint system and size, depending on the interface type, would be different. Instead, the identified joint (converged) for each interface type is recoupled to the blade and disk and compared with the reference FRF measurement which was not used in the identification process.

4.1 Translational DoF Interface

In an FRF testing, measuring translations are generally preferred but the interface lacks the rotational information. The rotations can be computed by the method of finite difference [18]. Alternatively, if sufficient translational DoF are present on the interface such that they are non-collinear, the rotational effect is indirectly included in the interface [19]. This is why the explicit inclusion of rotations at the interface in FE models with only translational DoF is not necessary. In the numerical models of the blade and disk, some translational DoF on the mating surfaces are selected as representative boundary DoF (Figure 3b and 3c)

(a) Interface nodes set {1,3,4,6}   (b) Interface nodes set {1,4,7,9}
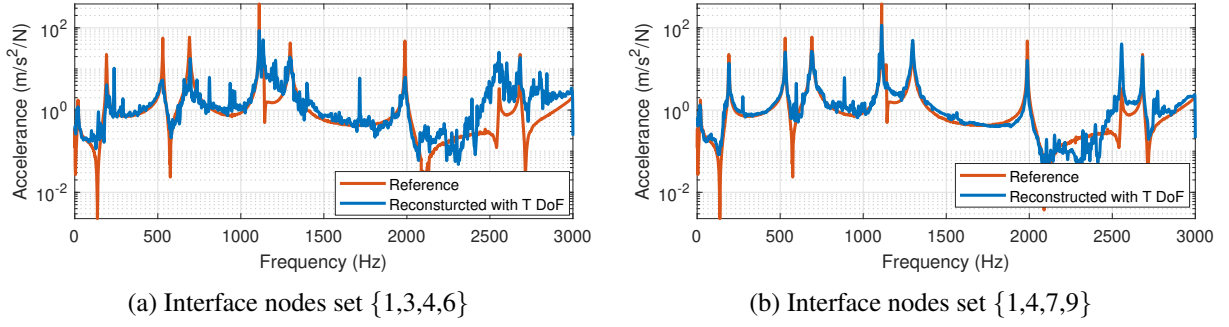
Figure 4: FRFs on the coupled blade-disk by considering only translational DoF at the interface. The reference FRF is measured at the locations shown in Figure 1b.

which are then expanded over in their respective hybrid models. Since the expansion is done by virtue of measurements on the internal DoF, it is assumed that these DoF can properly represent the interface DoF. However, it is not true for any arbitrary set of interface DoF, because different interface DoF combinations will produce different effects (to be discussed next).

It is seen in Figure 3a that the blade-root joint has three mating sides. A total of 27 translational DoF (9 nodes) are selected on these sides, indicated in Figure 3b and 3c. The nodes are shown only on the blade. Of course, a corresponding set is also selected on the disk interface. Among these nodes, multiple combinations can be tried. We examine only two cases of 12 DoF per substructure (24×24 joint model) here:

Case 1: Coupling of the DoF at nodes $\{1, 3, 4, 6\}$ – two physical nodes on the left and two on the right side, as shown in Figure 4a.

Case 2: Coupling of the DoF at nodes $\{1, 4, 7, 9\}$ – one physical node on the left, one on the right and two on the bottom, as shown in Figure 4b.

Remark 3. *Identification Rank: Since measurements on the assembled system have a rank of 27 (see Table 1), one can identify a joint with the same maximum rank. However, one or more channels are kept for validation and we allow for some over-fitting, the maximum rank of the joint system is set to be 24. That is, a 24×24 joint FRF matrix is identified.*

The reconstructed FRFs in blue in Figure 4 are obtained by recoupling the identified joint $\mathbf{Y}^J$ with the hybrid model of the blade $\mathbf{Y}^{S,A}$ and disk $\mathbf{Y}^{S,B}$. Note $\mathbf{Y}^J$ is retrieved after the convergence criterion has been met, as outlined in Section 2.4. Clearly, the interface of Case 1 has a lot of spurious effect even though it follows the shape of the reference FRF (orange colour in Figure 4a). This means that by considering only two sides of the interface, the joint is not properly identified. In Case 2, the third (bottom) side of the interface is taken into account through nodes 7 and 9. The reconstructed FRF overlaps the reference FRF well until 2000 Hz with the exceptional spurious peaks around 250, 600 and 800-1000 Hz. The response near anti-resonance of 600 Hz is also not accurately predicted. The reconstructed FRF of Case 2 is certainly better than that of Case 1 because the bottom side is thought to be a key location where the bolts are connected and push the blade to fit the other two surfaces of the disk. The interface seems to be better described by these locations and it gives an idea to consider these locations for further analysis. However, an interface defined by only the translational DoF of the two bottom nodes (7 and 9) would not be sufficient i.e. the other sides should also be considered.

4.2 Virtual Point Interface

In an interface defined only by the translational DoF, the selection of the corresponding nodes is an arbitrary choice of the user in terms of location (and numbers of nodes) involved in the identification. Therefore, many combinations are possible and it is not easy to understand what is the most promising combination.

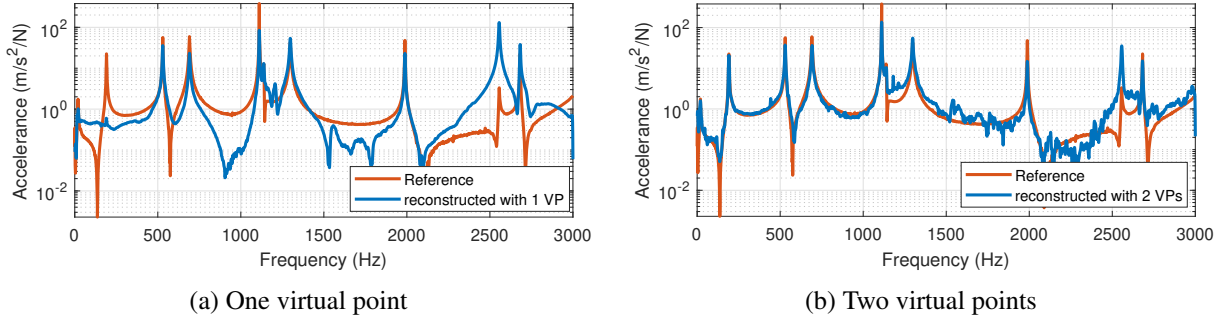(a) One virtual point   (b) Two virtual points

Figure 5: FRF of the blade-disk assembly coupled by the virtual interface descriptions. The reference FRF is measured at the locations shown in Figure 1b.

This problem can be overcome by creating a virtual interface characterized by both translations and rotations. All the measured or expanded translational DoF can then be used and projected to the virtual interface by least-squares [20]. Consider the hybrid model, for example, of the blade $\mathbf{Y}^{S,A}$ with the expanded dynamics on all the translational DoF $\mathbf{u}_b^A$ in Figure 3. The boundary translations $\mathbf{u}_b^A$ relate to the virtual displacements (translational and angular) $\mathbf{q}^A$ by:

$$\begin{Bmatrix} \mathbf{u}_i^A \\ \mathbf{u}_b^A \end{Bmatrix} = \underbrace{\begin{bmatrix} \mathbf{I} & \mathbf{0} \\ \mathbf{0} & \mathbf{R}_u^A \end{bmatrix}}_{\mathbf{R}^A} \begin{Bmatrix} \mathbf{u}_i^A \\ \mathbf{q}^A \end{Bmatrix} \tag{11}$$

where $\mathbf{R}_u^A$ contains the positions and orientations of the DoF in $\mathbf{u}_b^A$ with respect to the virtual point(s). The right hand side vector is obtained as:

$$\begin{Bmatrix} \mathbf{u}_i^A \\ \mathbf{q}^A \end{Bmatrix} = \underbrace{((\mathbf{R}^A)^T \mathbf{R}^A)^{-1} (\mathbf{R}^A)^T}_{\mathbf{T}_u^A} \begin{Bmatrix} \mathbf{u}_i^A \\ \mathbf{u}_b^A \end{Bmatrix} \tag{12}$$

A similar transformation $\mathbf{T}_f^A$ applies for the virtual forces and moments $\mathbf{m}^A$. If the DoF are collocated, as obtained by the hybrid models, $\mathbf{T}_u^A = \mathbf{T}_f^A = \mathbf{T}^A$. The new hybrid FRF matrix $\bar{\mathbf{Y}}^{S,A}$ with the virtual interface is calculated by

$$\bar{\mathbf{Y}}^{S,A} = \mathbf{T}^A \, \mathbf{Y}^{S,A} \, (\mathbf{T}^A)^T \tag{13}$$

For the virtual interface, we again consider two cases with two different configurations in which all the 27 expanded translational DoF are transformed to the VP(s) shown in Figure 3d and 3e, respectively. Note that the VP position can be defined even outside the structure, as long as the condition of rigid transformation holds.

Case 3: One virtual point (3 translations and 3 rotations per substructure). The joint is characterized by a 12×12 system, unlike Case 1 and Case 2.

Case 4: Two virtual points (6 translations and 6 rotations per substructure). The joint is characterized by a 24×24 system.

The respective reconstructed FRFs are plotted in Figure 5. In the FRFs of Case 3 (Figure 5a), not a good agreement is observed between the reconstructed and reference FRFs. This shows that an interface with 6 virtual DoF despite a least squares contribution from all the translational FRFs is not sufficient to capture the coupled system dynamics accurately. This dove-tail type joint needs a minimum set of interface DoF, also discussed numerically in [21]. This experimental investigation validates those findings.

The FRF obtained for Case 4 (two VPs) is shown in Figure 5b. The reconstructed FRF has certainly better agreement than that of Case 3. It is of more interest to compare this reconstructed FRF with that of Case

2 with translational DoF (Figure 4b). With the two VP interface, the identification resulted in i) a significantly reduced spurious effect up to 1100 Hz, ii) a better amplitude estimation on the resonances, iii) a good approach on the two anti-resonances around 150 and 600 Hz, and iv) slightly increased spurious effects between 1300 to 2000 Hz. The prediction beyond 2000 Hz is poor for both the cases. For practical purposes of low to medium frequency range, the two VP interface is considered to be a good choice and will be used in the following analyses.

5 Singular Value Filtering

In this section, the effect of singular values (SV) truncation (called SV filtering) while computing the pseudo-inverses is investigated in connection with the joint identification. In SEMM, the first use of SV filtering was made in [16] and applied to a numerical benchmark structure i.e. only a single uncoupled structure was considered. Here, it is applied to the two blade and the disk substructures and their direct effect on the joint identification is discussed. Let $\mathbf{P}$ denote one of the pseudo-inverses in Eq. (6). It can be decomposed into:

$$\mathbf{P} = \mathbf{U}\mathbf{S}\mathbf{V}^T \tag{14}$$

where $\mathbf{S}$ is a diagonal matrix containing singular values and $\mathbf{U}$ and $\mathbf{V}$ are unitary matrices of left and right singular vectors, respectively. The pseudo inverse can be computed by

$$\mathbf{P}^+ = \mathbf{V}\mathbf{S}^{-1}\mathbf{U}^T \tag{15}$$

If $\mathbf{u}_j$ and $\mathbf{v}_j$ represent jth vectors in $\mathbf{U}$ and $\mathbf{V}$, respectively, then Eq. (15) is written in the summation form:

$$\mathbf{P}^+ = \sum_j^N \mathbf{v}_j \sigma_j \mathbf{u}_j^T \approx \sum_j^{k<N} \mathbf{v}_j \sigma_j \mathbf{u}_j^T \tag{16}$$

where σ_j is the jth singular value in $\mathbf{S}^{-1}$ and N is the smallest dimension of $\mathbf{P}$. In this form, the contribution of each jth singular value is being computed. Thus, the smallest $N - k$ SVs can be filtered out without significantly affecting the inverse computation. Since $\mathbf{P}$, in general, is a frequency dependent matrix, the decomposition needs to be done at every frequency.

The use of SV filtering is motivated by looking at the blade's condition number of its experimental $\mathbf{Y}^{\mathrm{ov},A}$, numerical $\mathbf{Y}^{\mathrm{N},A}$ and hybrid models $\mathbf{Y}^{\mathrm{S},A}$ in Figure 6a. Condition number is defined as the ratio of the largest to the lowest singular value. In the figure, the peaks in the respective plots refer to the resonances. It is seen that the blade hybrid model has higher condition number (by 1-2 orders of magnitude) compared to the numerical and the experimental models throughout the frequency band. More importantly, the noise or measurement errors have propagated in the hybrid model from the experimental model in the range of 400-800 Hz. Since the hybrid model has a relatively larger set of DoF than the experimental model, the lowest singular values (supposedly corresponding to noise and insignificant dynamics) become even smaller, thereby, making the condition number high. So the SV filtering is justified in this case. By removing the two smallest SVs in the blade hybrid model, the new condition is lower and shows that the noise was attributed to the filtered SVs.

In the following, the SV filtered hybrid models of the blade and disk are used to identify the joint with the two VP interface. To see a significant effect, two SVs are filtered in each hybrid sub-model at a time i.e. if the SVs are filtered in the blade, the disk model is kept as such and vice versa. The corresponding validation FRFs are shown in Figure 7a and Figure 7b. They should be compared with the reconstructed FRFs of Figure 5b obtained by the unfiltered hybrid models. Since a good agreement up to 1100 Hz was observed with the unfiltered models, the attention is given to the frequency range greater than 1100 Hz. In the reconstructed FRF of Figure 7a, the identification by filtering in the blade has improved remarkably. The region between 1500–2000 Hz overlaps well with the reference FRF. The resonances around 2550 and 2700 Hz are also better estimated. The identification after the anti-resonance of 2100 Hz is also improved in comparison with that of Figure 5b, however, it still has some spurious effect. The low amplitude regions like
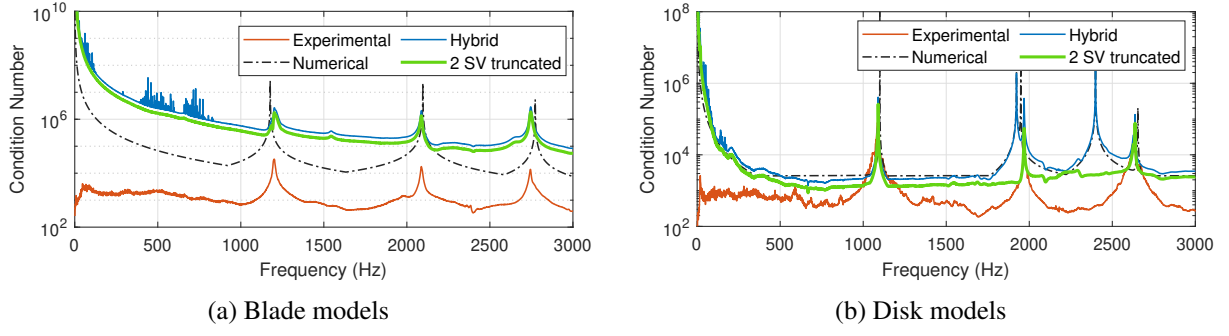
| (a) Blade models | (b) Disk models |

Figure 6: The condition number of the experimental, numerical and hybrid FRF matrices of (a) the blade and (b) the disk. In each hybrid model, the condition number by truncating two singular values is also plotted.

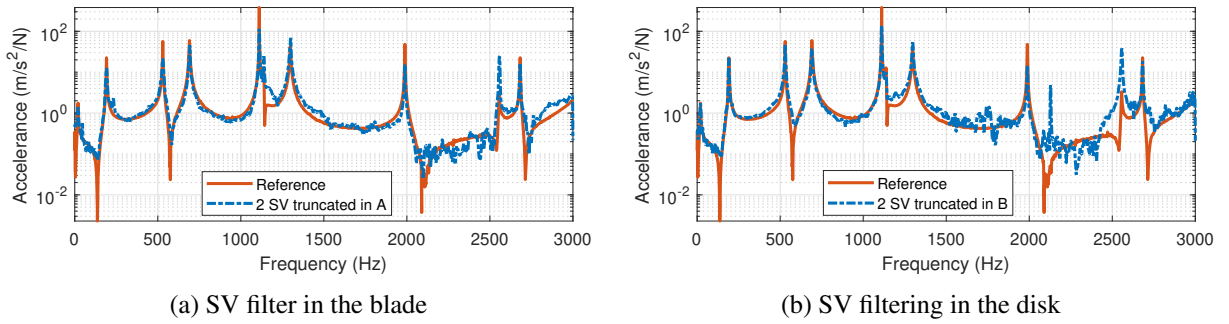| (a) SV filter in the blade | (b) SV filtering in the disk |

Figure 7: Effect of singular value filters on the recoupled system after joint identification. The filters are applied separately to the blade and disk. The reference FRF is measured at the locations shown in Figure 1b.

these are likely to get affected by the measurement errors. Despite this, it can be confidently said that the removal of the two lowest SVs in the blade hybrid model has appreciably improved the joint identification.

The SV filtering in the disk hybrid model has instead degraded the identification in the high frequency range, as evident in the FRF of Figure 7b. In order to understand the reasons, the condition number plots of the disk models are seen in Figure 6b. The disk's hybrid model's condition number is nearly of the same order as that of the numerical model and it is not as high as in the case of the blade (Figure 6a). By looking at the 2 SV truncated condition number (green plot) of the disk, there is a considerable change in the condition number pattern from its unfiltered hybrid model. This implies that the lowest filtered SVs are not very small and insignificant to be truncated. That is why, their filtration altered the disk hybrid dynamics.

From the above analysis, it is proposed that the SV filters should be deployed in the hybrid sub-models based on their condition number before and after filtering. If the condition number pattern of the filtered hybrid models is significantly different, the filtering may not affect positively on the joint identification.

Remark 4. *The SV filter is applied only to the substructures here i.e. while computing the hybrid FRF models of the blade and disk. One might consider to apply the same filter to the assembly's hybrid model in Eq. (8). If the SV filters are applied to the assembly, then recalling the iterative nature of the decoupling method from Eq. (7)–(9), the assembled system's dynamics in the hybrid model are updated at each iteration due to two factors: the updated joint and the modified paths [16, 22] for the measured dynamics in the assembly (due to filtered SVs). As a result, the convergence is not guaranteed for the joint identification. From another perspective, the system which we aim to identify is being modified at every iteration of the identification. This makes the filtration unwarranted on the assembled systems.*

6   Conclusions

In this paper, the joint dynamics are identified for a blade-root joint. The interface between the blade and disk is inaccessible for measurements. Thus, dynamics on the interface DoF have to be expanded. The authors had attempted to identify the joint dynamics in [11] using the SEMM expansion based decoupling method. However, the identified dynamics had restrictive accuracy. In this paper, we have investigated some of the key factors that affect the joint identification method by conducting a new set of measurement campaign in the free boundary conditions. This resulted in much better expanded FRFs on the disk.

The substructure coupling or decoupling has much to do with the way the interface is defined. An interface with only translational DoF (in a non-collinear fashion) was very selective and various combinations have to be tried until the best one is found. Even though the blade-root joint under consideration is three-faced, the significant dynamic contribution comes from the bottom side DoF where the bolts are mounted. However, it was not sufficient to consider only the translational interface at these DoF. All the expanded boundary dynamics were then transformed in a least-squares fashion to one or two virtual point type interface (translations and rotations), respectively. The one VP interface failed to identify the joint at all. However, the two VP interface could identify very well the dynamics up to 1100 Hz range as well as most of the resonances. This suggests that the minimum identification rank or joint size must be equivalent to two VP per substructure due to the number of independent measurements on the assembly. The two VP interface was then adopted so as to improve the prediction beyond 1100 Hz range by other factors.

The substructure hybrid models (blade and disk) are computed by a formulation of SEMM that allows for filtration based on the singular values (SV). The effect of SV filter on the substructure or joint identification is investigated for the first time. By filtering the two lowest SVs in the blade hybrid model, the joint identification improved significantly beyond 1100 Hz. On the other hand, the same filtering in the disk did not produce much anticipated result. To know whether the SV filtering would positively impact the joint identification, the pre- and post-filtering condition number can be computed. In the case of the disk, the pre-filtering condition number was not high unlike the blade. The filtering resulted in the change in condition number pattern over the entire frequency band.

In short, the joint identification in this study has been shown to improve by taking the following actions:

1. reducing the expansion error by removing the constraint modelling,

2. defining the two VP interface on the bottom side near the bolts

3. filtering two singular values in the blade hybrid model (none in the disk)

The challenge remains to more accurately predict the low amplitude regions which are easily influenced by errors and should be further investigated in the future.

Acknowledgements

References

[1] M. Krack, L. Salles, and F. Thouverez, "Vibration Prediction of Bladed Disks Coupled by Friction Joints," *Archives of Computational Methods in Engineering*, vol. 24, no. 3, pp. 589–636, 2017.

[2] Z. Saeed, G. Jenovencio, S. Arul, J. Blahoš, A. Sudhakar, L. Pesaresi, J. Yuan, F. El Haddad, H. Hetzler, and L. Salles, "A Test-Case on Continuation Methods for Bladed-Disk Vibration with Contact and Friction," in *Nonlinear Structures and Systems, Volume 1. Conference Proceedings of the Society for*

Experimental Mechanics Series, G. Kerschen, M. Brake, and L. Renson, Eds. Springer, Cham, 2020, pp. 209–212. [Online]. Available: http://link.springer.com/10.1007/978-3-030-12391-8{_}27

[3] S. N. Voormeeren and D. J. Rixen, "A family of substructure decoupling techniques based on a dual assembly approach," *Mechanical Systems and Signal Processing*, vol. 27, no. 1, pp. 379–396, feb 2012.

[4] W. D'Ambrogio and A. Fregolent, "Direct decoupling of substructures using primal and dual formulation," in *Conference Proceedings of the Society for Experimental Mechanics Series*, vol. 2, 2011, pp. 47–76.

[5] S. W. Klaassen, M. V. van der Seijs, and D. de Klerk, "System equivalent model mixing," *Mechanical Systems and Signal Processing*, vol. 105, no. December, pp. 90–112, 2018. [Online]. Available: https://doi.org/10.1016/j.ymssp.2017.12.003

[6] J. S. Tsai and Y. F. Chou, "The identification of dynamic characteristics of a single bolt joint," *Journal of Sound and Vibration*, vol. 125, no. 3, pp. 487–502, 1988.

[7] Y. Ren and C. F. Beards, "Identification of 'effective' linear joints using coupling and joint identification techniques," *Journal of Vibration and Acoustics, Transactions of the ASME*, vol. 120, no. 2, pp. 331–338, 1998.

[8] J. Zhen, T. C. Lim, and G. Lu, "Determination of system vibratory response characteristics applying a spectral-based inverse sub-structuring approach. Part I: analytical formulation," Tech. Rep. 2, 2004.

[9] e. Tol and H. N. Özgüven, "Dynamic characterization of bolted joints using FRF decoupling and optimization," *Mechanical Systems and Signal Processing*, vol. 54, pp. 124–138, mar 2015.

[10] S. W. Klaassen and D. J. Rixen, "Using SEMM to Identify the Joint Dynamics in Multiple Degrees of Freedom Without Measuring Interfaces," in *Conference Proceedings of the Society for Experimental Mechanics Series*, 2020, pp. 87–99.

[11] Z. Saeed, S. W. B. Klaassen, C. M. Firrone, T. M. Berruti, and D. J. Rixen, "Experimental Joint Identification Using System Equivalent Model Mixing in a Bladed Disk," *Journal of Vibration and Acoustics*, vol. 142, no. 5, jun 2020. [Online]. Available: https://doi.org/10.1115/1.4047361

[12] D. De Klerk, D. J. Rixen, and S. N. Voormeeren, "General framework for dynamic substructuring: History, review, and classification of techniques," *AIAA Journal*, vol. 46, no. 5, pp. 1169–1181, 2008. [Online]. Available: http://arc.aiaa.org/doi/10.2514/1.33274

[13] D. J. Rixen, "How measurement inaccuracies induce spurious peaks in Frequency Based Substructuring," in *Conference Proceedings of the Society for Experimental Mechanics Series*, 2008.

[14] W. D'Ambrogio and A. Fregolent, "Are rotational DoFs essential in substructure decoupling?" in *Conference Proceedings of the Society for Experimental Mechanics Series*, vol. 1. Springer New York LLC, 2014, pp. 27–36.

[15] A. Drozg, G. Čepon, and M. Boltežar, "Full-degrees-of-freedom frequency based substructuring," *Mechanical Systems and Signal Processing*, vol. 98, pp. 570–579, jan 2018.

[16] S. W. B. Klaassen and D. J. Rixen, "The inclusion of a singular-value based filter in SEMM," in *International Modal Analysis Conference*, Houston, Texas, 2020, pp. 1—-15.

[17] D. De Klerk, D. J. Rixen, and J. De Jong, "The Frequency Based Substructuring (FBS) method reformulated according to the dual Domain Decomposition method," in *Conference Proceedings of the Society for Experimental Mechanics Series*, 2006.

[18] M. L. M. Duarte and D. J. Ewins, "Rotational degrees of freedom for structural coupling analysis via finite-difference technique with residual compensation," *Mechanical Systems and Signal Processing*, vol. 14, no. 2, pp. 205–227, mar 2000. [Online]. Available: https://www.sciencedirect.com/science/article/pii/S0888327099912414

[19] D. De Klerk, D. J. Rixen, S. N. Voormeeren, and F. Pasteuning, "Solving the RDoF problem in experimental dynamic substructuring," Tech. Rep., 2008.

[20] M. V. Van Der Seijs, D. D. Van Den Bosch, D. J. Rixen, and D. De Klerk, "An improved methodology for the virtual point transformation of measured frequency response functions in Dynamic Substructuring," in *ECCOMAS Thematic Conference - COMPDYN 2013: 4th International Conference on Computational Methods in Structural Dynamics and Earthquake Engineering, Proceedings - An IACM Special Interest Conference*. ECCOMAS, apr 2013, pp. 4334–4347.

[21] Z. Saeed, C. M. Firrone, and T. M. Berruti, "Substructuring for Contact Parameters Identification in Bladed-disks," *Journal of Physics: Conference Series*, vol. 1264, no. 1, p. 012037, jul 2019. [Online]. Available: https://iopscience.iop.org/article/10.1088/1742-6596/1264/1/012037

[22] M. V. van der Seijs, "Experimental Dynamic Substructuring Analysis and Design Strategies for Vehicle Development," Ph.D. dissertation, Delft University of Technology, 2016.